



Delft University of Technology

Development and Performance of the 10 kN Hybrid Rocket Motor for the Stratos II Sounding Rocket

Werner, Robert; Knop, Tobias; Wink, J; Ehlen, J; Huijsman, R; Powell, S; Florea, R.; Wieling, W; Cervone, Angelo; Zandbergen, Barry

Publication date

2016

Document Version

Accepted author manuscript

Published in

Space propulsion 2016

Citation (APA)

Werner, R., Knop, T., Wink, J., Ehlen, J., Huijsman, R., Powell, S., Florea, R., Wieling, W., Cervone, A., & Zandbergen, B. (2016). Development and Performance of the 10 kN Hybrid Rocket Motor for the Stratos II Sounding Rocket. In *Space propulsion 2016* Article SP2016-3124672

Important note

To cite this publication, please use the final published version (if applicable). Please check the document version above.

Copyright

Other than for strictly personal use, it is not permitted to download, forward or distribute the text or part of it, without the consent of the author(s) and/or copyright holder(s), unless the work is under an open content license such as Creative Commons.

Takedown policy

Please contact us and provide details if you believe this document breaches copyrights. We will remove access to the work immediately and investigate your claim.

DEVELOPMENT AND PERFORMANCE OF THE 10 kN HYBRID ROCKET MOTOR FOR THE STRATOS II SOUNDING ROCKET

Robert Werner¹, Tobias Knop², Jeroen Wink¹, Johannes Ehlen¹, Ralph Huijsman¹, Stefan Powell², Radu Florea¹, Wolter Wieling³, Angelo Cervone⁴ and Barry Zandbergen⁵
Corresponding adress: r.m.werner@student.tudelft.nl

¹ Msc. Student Aerospace Engineering, Delft University of Technology, Delft, The Netherlands ² Graduated Msc. Student Aerospace Engineering, Delft University of Technology, Delft, The Netherlands ³ Msc. TNO-PML, The Hague, Delft, The Netherlands ⁴ Assistant Professor Aerospace Engineering, Delft University of Technology, Delft, The Netherlands ⁵ Senior lecturer Aerospace Engineering, Delft University of Technology, Delft, The Netherlands

ABSTRACT

This paper presents the development work of the 10 kN hybrid rocket motor DHX-200 Aurora. The DHX-200 Aurora was developed by Delft Aerospace Rocket Engineering (DARE) to power the Stratos II and Stratos II+ sounding rocket, with the later one being launched in October 2015. Stratos II and Stratos II+ are the flagship projects of DARE, a student group working on rocketry at Delft University of Technology. Successors of Stratos II have the eventual goal of reaching space.

During the development process two major revisions of the motor have been designed with smaller changes between tests. The second major design revision was made after a first test series showed low combustion efficiency, through the usage of a CFD model to improve mixing. Both revisions have been tested statically in total for 14 times both at facilities of 'Nederlandse Organisatie voor Toegepast Natuurwetenschappelijk Onderzoek' (TNO) and 'Deutsches Zentrum für Luft- und Raumfahrt' (DLR). All tests were conducted in a full-scale, flight-ready configuration with the primary goal of demonstrating the required performance for the Stratos II and Stratos II+ sounding rocket. It was found out that the motor suffered from combustion instabilities at around 450 Hz, when operated at its design oxidizer mass flux level of $600 \text{ kg/m}^2/\text{s}$, that caused low combustion efficiency and elevated heat flux levels in the pre-combustion chamber. Through design changes the instabilities could be lowered and both problems removed. The design goal of total impulse could not be met, but the specific impulse measured was higher than expected. Still, the overall performance proofed to be sufficient enough for the system to be used as the propulsion system for Stratos II+.

NOMENCLATURE

I_{sp}	Specific Impulse at sea level, [s]
O/F	Oxidizer-to-fuel mass ratio, [-]
\dot{m}	mass flow, [kg/s]
p_c	Chamber pressure
A_t	Area of nozzle throat
η	Motor efficiency [%]
ρ	Density, [kg/m ³]
c^*	Experimental Characteristic Velocity, [m/s]

Subscripts

num	numerical value
$ideal$	ideal value

1 INTRODUCTION

Delft Aerospace Rocket Engineering (DARE) is an organization of students from Delft University of Technology. Its members are full time students from different faculties who design, construct, test and launch sounding rockets as an extracurricular activity. In 2009, DARE broke the European altitude record for amateur rockets with the launch of Stratos I to 12.5 km [11]. Stratos I was powered by a two-stage, sorbitol and potassium nitrate solid rocket propulsion system.

This record was unchallenged until in October 2015 the successor mission, Stratos II+, was launched to an altitude of 21.5km beating that record [12]. The year before, a launch attempt was made using Stratos II, that did not succeed due to a frozen main oxidizer valve [5]. Stratos II+ features a single-stage hybrid rocket motor designed to deliver a 15 kg scientific payload to an apogee of 50 km. Stratos II+ requires a propulsion system capable of delivering approximately 10 kN of thrust and 200 kNs of total impulse. Scaling up the propulsion

system of Stratos I was considered infeasible due to the low specific impulse of 110 s of DARE's traditional solid rocket motors. To overcome this limitation, a team for the development of an alternative propulsion concept was established in 2010 by a group of international students within DARE [4]. Since the low regression characteristics of traditional hybrid rocket fuels like Hydroxyl Terminated Polybutadiene (HTPB) often lead to multi port designs with low volumetric efficiency and high sliver fractions, it was decided that a new fuel was to be developed [10]. Sorbitol was selected as a baseline due to the previous experience in handling within DARE and its experimentally proven regression rate in excess of the mentioned traditional fuels [2]. Furthermore, it also offers a high mass density of 1489 kg/m^3 , a low ideal O/F ratio of 3 and it can be cast. After a series of fuel characterization tests, it was found that the addition of 10 % paraffin and 10 % aluminium to the sorbitol baseline yielded combustion characteristics sufficient for the requirements of the Stratos II+ sounding rocket [7]. After the characterization tests on a 1000 Ns test motor, a 200 kNs motor, the DHX-200 Aurora, was designed as the motor of the Stratos II+ sounding rocket.

A series of tests have been performed on this motor in a flight configuration to characterize its performance [13]. In total 14 tests were conducted at both 'Nederlandse Organisatie voor Toegepast Natuurwetenschappelijk Onderzoek' (TNO) and 'Deutsches Zentrum für Luft- und Raumfahrt' (DLR). During these tests two distinctive failure modes were encountered and design changes have been implemented to mitigate these failures [8]. Additionally, further changes have been implemented based on the data collected from the tests and additional fluid simulations, to both increase the performance as well as the combustion stability. This paper describes the original design of the motor as well as the subsequent changes and the rationale for implementation. From the hotfire tests conclusions are drawn on the effectiveness of the changes and recommendations are given on future implementations.

2 METHODOLOGY

As part of the Stratos II+ project, the DHX-200 Aurora was designed to fulfil the mission requirements for this project. To accommodate these, the needed motor characteristics were deduced from the top-level requirements of the Stratos II+ project. Furthermore, certain constraints were imposed onto the design [7]. In preparation of this project a fuel characterisation study was performed on a lab scale sized motor. As a result the

80-10-10, sorbitol, paraffin, aluminium fuel blend, with a demonstrated Isp of 195 s, was chosen [7]. With the known fuel performance and the top-level requirements of carrying a payload of 15 kg to an altitude of 50 km, the needed impulse could be found through first order simulations and was set to 200 kNs (sea-level). For the thrust level multiple constraints existed, for aerodynamic reasons the rocket needed to lift off with at least 3 g. On the other end of the spectrum it was decided to not exceed a maximum oxidizer mass flux of $650 \frac{\text{kg}}{\text{m}^2\text{s}}$ to not experience flame holding instabilities [14]. Therefore 10 kN as the average thrust level was chosen.

With these parameters set a first prototype was designed and tested in a first test series of five tests. For the second test series of another five tests the internal ballistics of the motor were altered to improve mixing and thus achieve a higher efficiency. The applied changes on the post combustion chamber were based on CFD simulations performed on the motor. Furthermore, the pre combustion chamber was changed to provide additional thermal protection.

For the last test series of four tests changes on the injection and the pre combustion chamber were carried out to improve the stability of the combustion, based on data from previous tests. Due to difficulties in acquiring a suitable test locations all test series needed to be carried out within a small time frame of one-two weeks each with a break of multiple months in between. This led to limited abilities for analysis and design changes throughout a test series and only allowed for more substantial changes to be done between series without additional acceptance testing.

3 MOTOR

The motor has been designed to deliver a nominal thrust of 10 kN at a chamber pressure of 30 bar. As an initial oxidizer mass flux $630 \frac{\text{kg}}{\text{m}^2\text{s}}$ was chosen, to on the one side not experience flame holding instabilities [14] and on the other side to still achieve a high packaging factor of the grain (77.6%). Due to data gathered from testing this value has been changed after test 13 to $456 \frac{\text{kg}}{\text{m}^2\text{s}}$, by reducing the amount of injector holes, to avoid the onset of combustion instabilities, see also Sec.3.1 and Sec.7. The combustion chamber is a 5 mm walled aluminium, Al 6082-T6 tube with an inner diameter of 190 mm. All components share this diameter and are stacked inside the combustion chamber with radial tolerances of up to 0.2 mm. The 80% sorbitol, 10% paraffin, 10% aluminium powder (wrt. mass) single port fuel grain has an initial port diameter of 90 mm and a web thickness of 47 mm. The fuel is cast into a

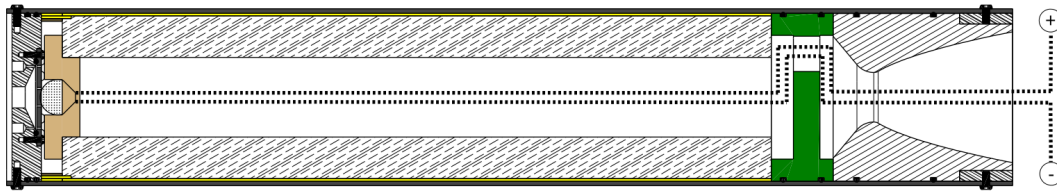


Figure 1: Schematic of the final design of the combustion chamber

3 mm cardboard liner, which aids in handling, adds minor structural support and also provides ablative cooling protection to the chamber wall once the fuel is burnt out. An ablatively cooled pre-combustion chamber between the injector and the fuel grain provides a recirculation area for flow vortices to form, providing flame holding at the forward end of the grain to increase the combustion stability and efficiency [6]. At the aft side of the fuel grain a post-combustion chamber mixing device is placed to enhance the combustion efficiency and stability [9]. The shape and material of this device has changed after the fifth test firing, a reasoning on the changes can be found under 4. The bell shaped nozzle is made from a single piece of medium density graphite and is held in place by an aluminium retainer ring which is fastened to the combustion chamber wall. The nozzle has a throat diameter of 56.4 mm and an area ratio of 6.5. The nozzle is sealed with a double o-ring seal and high-temperature silicone sealant. A drawing of the motor in the final configuration can be found in Fig. 1. Note, that there have been more iterations than presented, however, these were focused on fixing issues not related to performance, such as improvements on thermal protection and will not be treated in this paper. A thorough presentation on the aforementioned changes can be found in [8]. A comprehensive list of the design values can be found in Tab.3.

3.1 Injector

Nitrous oxide passes through a manifold, to which an interchangeable 5 mm thick aluminium injector plate is attached. The cylindrical orifices of the injector plate have a diameter of 1.5 mm and an injection angle of 15°

4 EFFICIENCY OPTIMIZATION USING CFD

The internal motor geometry of the first design iteration, which was used for tests 1-5 was purely based on first order sizing and experiences from preceding small scale test articles. With the order of 75% the combined motor efficiency was however far below the desired value of 90% [13].

For subsequent tests the internal geometry, more specifically the post-combustion chamber device, was

with respect to the longitudinal axis. Earlier studies have confirmed that this injector type will increase the mixing of the nitrous oxide with the fuel and hence increases regression rate [7]. The number of injector ports changed during the test campaign to compensate for previous modelling uncertainties that initially incorrectly predicted the mass flow rate to match the design value. During later tests instabilities were found that made it necessary to reduce the amount of injector holes from 92 to 72.

3.2 Igniter

The motor is ignited through a pyrotechnic squib supported with three grams of black powder and wrapped in steel wool. The igniter is held in place in the pre-combustion chamber by means of a balsa wood housing which is ejected from the motor during ignition. Balsa wood is used as it is unlikely to cause damage to the graphite nozzle when it is ejected at high velocity. An additively manufactured housing made from PLA (polylactic acid) has been tried previously and proved to be unreliable. Due to the heat the housing lost its structural properties and enabled the burning steel wool to slide to the nozzle end of the combustion, failing to properly ignite the motor. Four seconds before the motor is ignited, the motor is primed with a small flow (30 g/s) of nitrous oxide and the igniter is fired. This small nitrous oxide flow ignites and burns the steel wool at near-ambient pressure, pre-heating the combustion chamber and the fuel grain surfaces. When the main oxidizer valves opens, the pre-heated motor is completely ignited. This technique is used, as it ensures smooth and fast motor start up behaviour.

optimized by using a computational fluid dynamics approach. The computational approach itself was required to be run on office PCs and yield qualitative results on several candidate shapes for post-combustion chamber devices. The methodology used trades computational time in favour of absolute result accuracy and explicitly excludes on-line shape optimization.

The method selected has previously been applied to hybrid rocket motors [1]. It features a single forward

reaction equation, gaseous injection of the oxidiser at comparable injection velocities, radial gaseous injection of fuel, which is assumed to be composed of the already decomposed products of the actual fuel and a steady-state solution on a single grain and post-combustion chamber device geometry. The simulation itself is run in ANSYS CFX.

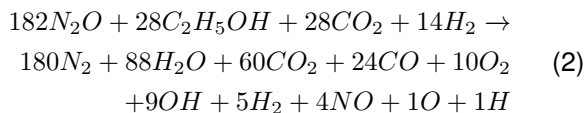
While the DHX-200 Aurora utilizes liquid nitrous oxide as its oxidiser the model injects the nitrous oxide in gaseous phase. In light of limited time and available computational power the modelling effort of liquid injection including droplet break-up was considered to be unnecessarily complex for a comparative study of post-combustion chamber devices. In the model the gaseous nitrous oxide is injected in a swirling, homogeneous stream through a single, large bore opening that resembles the injector face covered with injector ports. The swirl angle is identical to the experimental injector 15° with respect to the motor center axis. Through the increased injection area of the representative single bore injector and the decreased density of nitrous oxide vapour as compared to liquid a representative injection velocity is achieved.

The sorbitol fuel is injected in gaseous phase radially through the inner face of the fuel grain. In order to simplify implementation into the model the fuel is assumed to already be decomposed and vaporized into the gaseous constituents ethanol, carbon dioxide and hydrogen gas at a temperature of 700 K. The effects of aluminium and paraffin additives used in the test article have been neglected. According to stoichiometry the decomposition of the sorbitol fuel is assumed to be:



This results in a composition by mass of 50.6% ethanol, 48.3% carbon dioxide and 1.1% hydrogen gas.

The single forward reaction used in the simulation is based on the reaction product distribution found by NASA's CEA2 code for the design operating point. Reaction products contributing less than 0.1% to the total are omitted. In order to achieve stoichiometry using integer molar quantities errors up to 27% (NO, O, H) and up to 3.5% (all remaining constituents) with respect to the CEA2 results are accepted. Equation 2 shows the single reaction used in the simulation.



A $k-\epsilon$ turbulence model is used as well as an eddy dissipation model for the combustion. Inlet boundary

conditions are defined by fixed mass flow through the oxidizer injector at 3.9 kg/s of nitrous oxide and radial inner surface of the fuel grain at 1.3 kg/s of the described fuel mixture. This represents the design operating point of the motor. In order to save computational time, fractions of the combustion chamber combined with continuity boundary conditions have been applied wherever post-combustion chamber device symmetry allowed (Figure 2). The mesh used is a simple unstructured mesh of tetrahedrons with a maximum element size of 3.3 mm. A mesh refinement of 2.4 mm is used on all faces belonging to the grain and post-combustion chamber device. Eight inflation layers are used on all walls. The initial layer thickness is 0.1 mm with a growth rate of 1.2 (Figure 3). The resulting number of elements varies per exact configuration is however in the order of 1.2 million.

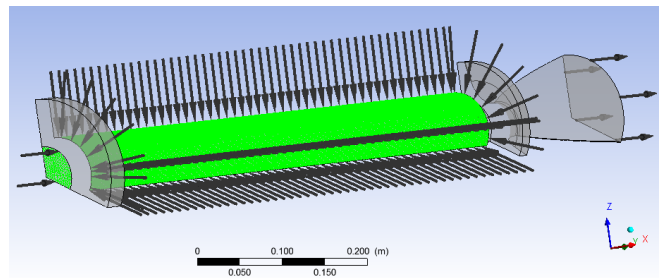


Figure 2: Boundary conditions of a generic 120° fluid shape section.

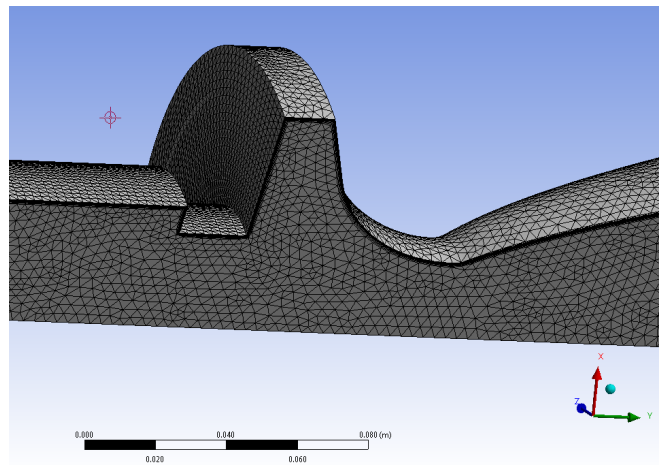


Figure 3: Close-up of the mesh at the post-combustion chamber (120° section).






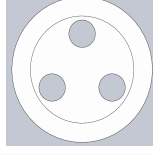
Seven basic post-combustion chamber device shapes that had been proposed based on first-order mixing behaviour, thermal and manufacturing aspects were compared using the numerical simulation. Main metric for comparison was the achieved combustion efficiency. The efficiency was evaluated by comparing the achieved

characteristic velocity (Equation 3) to the characteristic velocity determined by CEA2 (Equation 4). Here c_{num}^* and c_{ideal}^* are the characteristic velocities obtained by numerical simulation and equilibrium thermochemistry respectively, p_c is the combustion pressure evaluated at the nozzle inlet plane, A_t is the throat area defined by the nozzle geometry, \dot{m} is the total mass flow rate defined by the model inlet conditions, and η_{comb} is the resulting combustion efficiency. The basic shapes and results are presented in Table 1.

$$c_{num}^* = \frac{p_c \cdot A_t}{\dot{m}} \quad (3)$$

$$\eta_{comb} = \frac{c_{num}^*}{c_{ideal}^*} \quad (4)$$

Table 1: All simulated post-combustion chamber devices with resulting c^* efficiency (ideal $c^* = 1520$ m/s)

ID	Shape	η_{comb} achieved
1	no mixer	87.2 %
2		79.1 %
3		84.0 %
4		87.3 %
5		87.6 %
6		91.4 %
7		92.4 %

Notably the baseline shape used for the first five hot fires with a single circular hole performs worst. Even

omitting the post-combustion chamber device altogether results in a better performance than the baseline design. The winning design turned out to be shape number 7. The highest-ranking design conveniently also shows good manufacturability due to its simple shape.

While the simplifications and assumptions made during the modelling process are arguably compromising absolute accuracy of the modelling process, the related errors are introduced into all seven simulations. Comparison of the results in a relative sense still yields valuable insight and supports design decisions.

Later experimental results of the selected post-combustion chamber device would support this modelling approach in achieving significantly higher specific impulse, increasing up to 20% over the baseline.

5 EXPERIMENTAL SETUP

5.1 Test setup

The test stand consists out of a separate thrust bench and a tank holding rig (see Fig. 4). Both parts can be moved easily and are bolted onto the test chamber floor.

On the thrust bench the motor is bolted onto a carrier plate which is supported by flexible plates, from the rest of the thrust bench that only allows motion along a single axis. The forces along this axis are then taken up by a s-type load cell.

The tank holding rig consists out of two cylindrical tanks with an individual length of 2 m, that are vertically suspended in a truss structure. Furthermore, it features a beam type load cell that allows constant monitoring of the tanks weights. The tanks are made out of Al 6082-T6 with an outer diameter of 200 mm and a wall thickness of 5 mm, the same tubes the Stratos II rocket was constructed off. It was chosen to split up the 4 m tank of the rocket into two separate tanks of 2 m for static testing due to limited ceiling heights at both test locations. The tanks, or run tanks, are filled prior flight from commercially available nitrous oxide cylinders. The tanks are interconnected both at the top and the bottom to create a communicating vessel and simulate as closely as possible the actual tank of Stratos II. In total the tanks have a volume of 110 l and are designed to contain 80 kg of nitrous oxide at a pressure of 60 bar. The system is always kept at vapour pressure, for controlling the pressure a heating cable is wrapped around both tanks that can be activated remotely from the command post. If needed the pressure inside can be lowered by opening a valve located on top of the tanks (BV-1). For safety reasons additional safety valves are located on top of the tanks in case the pressure rises unexpectedly above 70 bar.

5.2 Feed system

In Fig. 6 an overview of the feed system can be found. The run tanks are connected via a pneumatically actuated ball valve (FV-1) to four 50 l nitrous oxide cylinders and filled by creating a differential pressure using the bleed valve (BV) on top of the run tanks. For ignition the chamber is primed with nitrous oxide using the solenoids IV-1 and IV-2. Both are actuated simultaneously and used in series to mitigate the risk of unintentional actuation. The main oxidizer flow is controlled by MV-1, a servo powered ball valve. In series with this valve is MV-2, a pneumatically actuated ball valve that is used for emergency shut downs and arming the system prior testing.

Additionally, two nitrogen bottles are connected to the system. The smaller one is used for powering actuators, whereas the larger one is used for purging and leak testing of the system.

5.3 Instrumentation

In order to properly assess the motor's performance, several sensors are incorporated into the test setup. In total there are two load cells (LC), four pressure sensors (DPS) and four thermocouples (TC). The placement of these sensors is shown in Fig. 5. The load cells are used to measure the tank mass (LC-1), and the thrust (LC-2). For the tank mass a 2 kN Tedeo-Huntleigh load cell (model 1240) is used, and for the thrust a 50 kN AST Force Transducer is used. The four pressure sen-

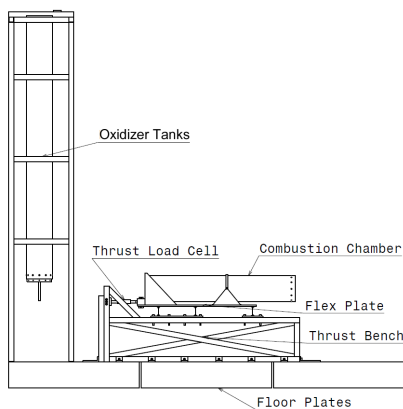


Figure 4: Side View of Test Assembly

sors, all of type Parker ASIC 0 - 100 bar, measure the pressure in the tank (DPS-1), the combustion chamber pressure (DPS-2), the injector manifold pressure (DPS-3), and the main oxidizer feed line pressure, just before the main valve (DPS-4). Due to a unification of different data acquisition systems into one system powered by a NI CompactRIO the sampling rates changed after test 6. A comprehensive list of the achievable resolutions and sampling rates can be found in table 2. Thermocouples of type K measure the temperature of the combustion chamber wall at the pre-combustion chamber (TC-1), post combustion chamber (TC-2) and the nozzle (TC-3 and TC-4).

5.4 Test plan

To evaluate the performance of the motor a test logic was devised, starting off with short burns to evaluate combustion characteristics, oxidizer mass flow and identifying heating problems early on. It was planned for full duration tests to follow up on the initial tests. The first test series has been planned to be a succession of a 5 s, a 10 s, a 15 s and a full duration test. The following tests were all planned as full duration burns, for the evaluation of the full system performance and for solving an issue caused by excessive heating of the pre-combustion chamber.

All tests were planned to be conducted under the same conditions, with a new and complete fuel grain and a completely filled oxidizer tank, that was heated to be at a vapour pressure of 60 bar.

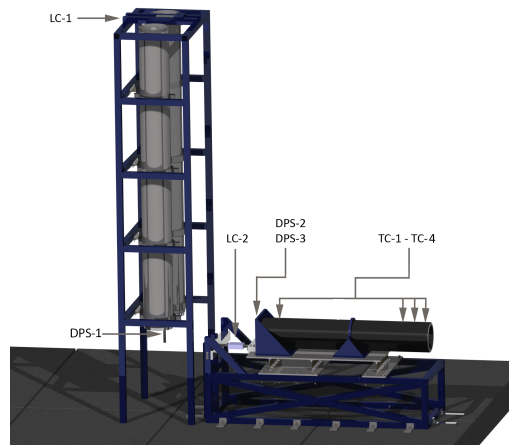


Figure 5: Test Bench Sensor Outline

Table 2: Sensors and their specifications.

Parameter	Sensor	Resolution	Sampling Rate (Test numbers)
Thrust	AST Force Transducer KAS 50kN	50 N	180 Hz (1-5) 1 kHz (6-10) 2kHz (11-14)
Run tank mass	Tedea-Huntleigh 1240 load cell 2 kN	0.4 N	180 Hz (1-5) 1 kHz (6-14)
Chamber pressure	Parker ASIC 0 - 100 bar	0.2 bar	2.2 kHz (1-5) 1 kHz (6-10) 2 kHz (11-14)
Other Pressures	Parker ASIC 0 - 100 bar	0.2 bar	180 Hz (1-5) 1kHz (6-10) 2kHz (11-14)

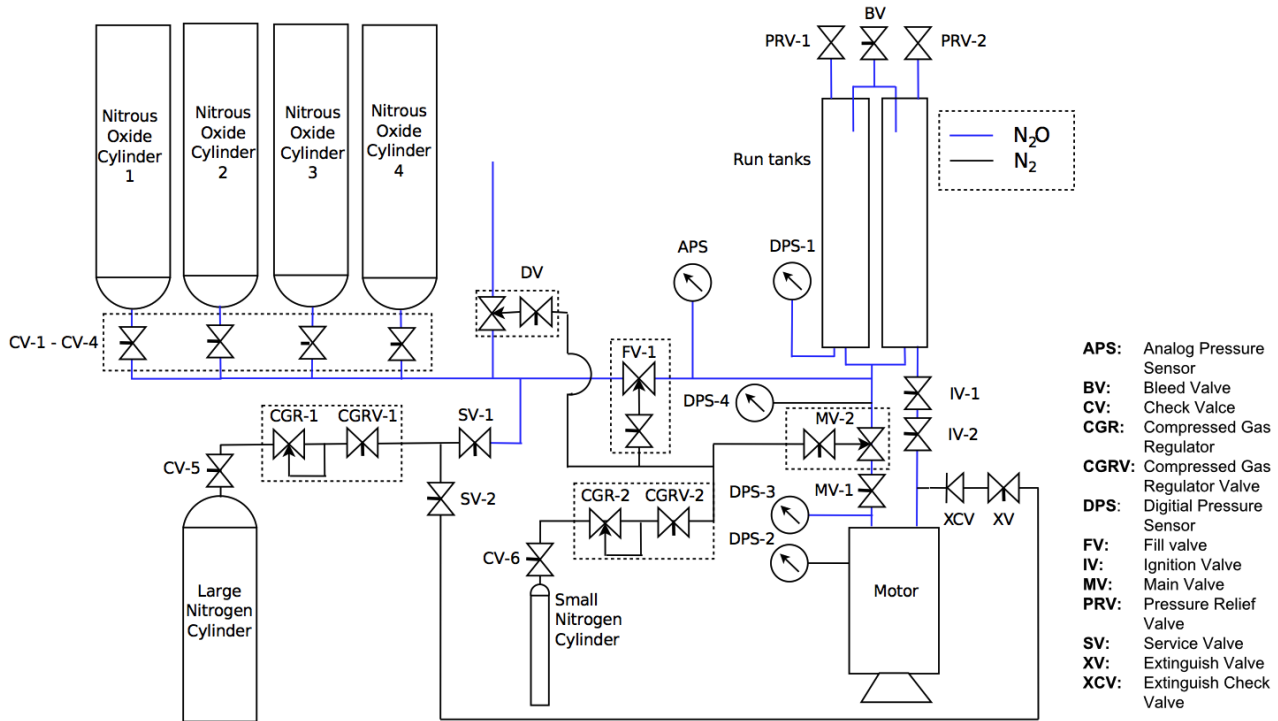


Figure 6: Test Setup Feed System Schematic

6 RESULTS

During the development a total of 14 test firings have been performed. In the following section an overview of these tests and the made changes is given, with an emphasis on the results of test 14, as this test featured the final configuration. Tests 1 and 2 successfully burned for their designed burn time, namely 5 and 10 seconds. Test 3 and 4 both suffered from a mid-grain failure of the combustion chamber wall after approximately 5 seconds caused by a cracking fuel grain [8]. The issue was fixed but test 5 resulted in a misfire due to a faulty ignition valve assembly. After test 5 the mixing device was changed, see 4. Test 6 successfully lasted for the planned 25 seconds. Tests 7,8 and 9 however all suffered a mechanical failure of the pre-combustion chamber wall after approximately 5 seconds. Test 10 suffered a failure near the nozzle after approximately 10

seconds. Test 11 featured a new igniter housing made from PLA that melted prematurely and led to an improper ignition. Test 12 and 13 showed the same failure mode as tests 7,8 and 9. Test 14 performed as planned but burned through after 23 s, as all the fuel was consumed due to too much oxidizer loaded into the run tanks.

In the following part an example thrust curve for each motor revision is presented, to give an overview over the achieved results. Test 2 represents the original design before the mixing device was updated, Test 6 represents a full burn with persistent (but low intensity) instabilities. Key performance parameters of these tests are also found in Tab. 3. Furthermore, a spectrogram of the combustion chamber pressure is given for Test 12 in Fig. 12 and for Test 14 in Fig. 13, the relative intensity is given by a colour scale from blue (low) to red (high).

Additionally, the combustion chamber, injector man-

ifold, feed system and tank pressures are presented in Fig 11, as test 14 represents the final configuration and is thus the most interesting.

It should be noted that because a blow-down system is characterized the oxidizer mass flow and thus the operating point shifts throughout the burn. It was therefore decided to use the systems specific impulse over the

whole burn as a measure of efficiency, as this parameter was the most relevant for the development. Due to the difficulty in determining the instantaneous mass flow of the fuel, the c^* value could also only be calculated over the whole burn and thus delivered no additional insights over the specific impulse. It is therefore omitted from this analysis.

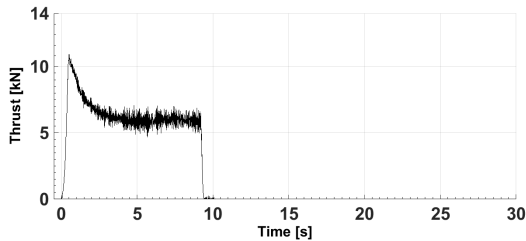


Figure 7: Thrust curve of test 2

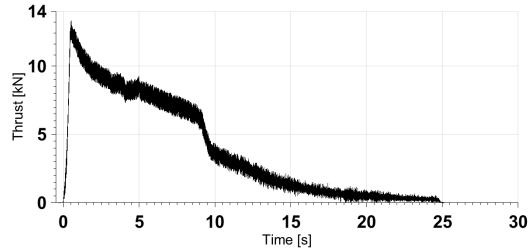


Figure 8: Thrust curve of test 6

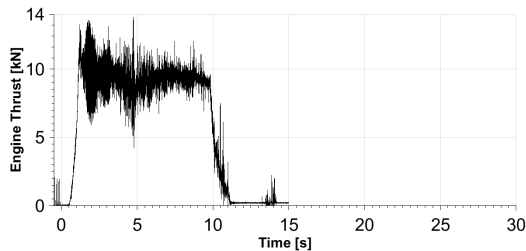


Figure 9: Thrust curve of test 12

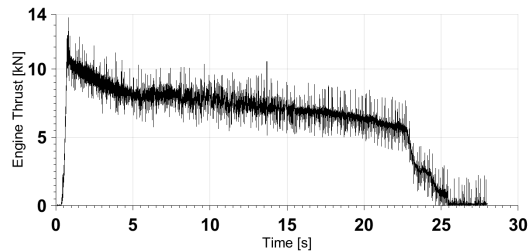


Figure 10: Thrust curve of test 14

	Test2	Test 6	Test 12	Test 14	Design
Peak Thrust [kN]	10	13	12.5	11	10
Average Thrust [kN]	6.4	8	9.8	7.8	10
Total Impulse [kNs]	58.75	98	88	177	200
Average oxidizer mass flow rate [kg/s]	2.95	3.4	3.44	2.9	4
Average Chamber pressure [bar]	21	13.6	N/A	23.3	30
ISP [s]	166	165	N/A	197	195
O/F	2.95	2.6	N/A	2.8	3.3

Table 3: Overview of key performance parameters at sea level

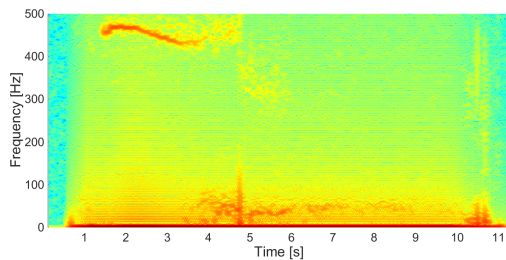


Figure 12: Spectrogram of the combustion chamber pressure for Test 12

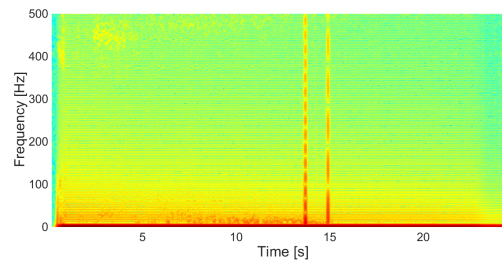


Figure 13: Spectrogram of the combustion chamber pressure for Test 14

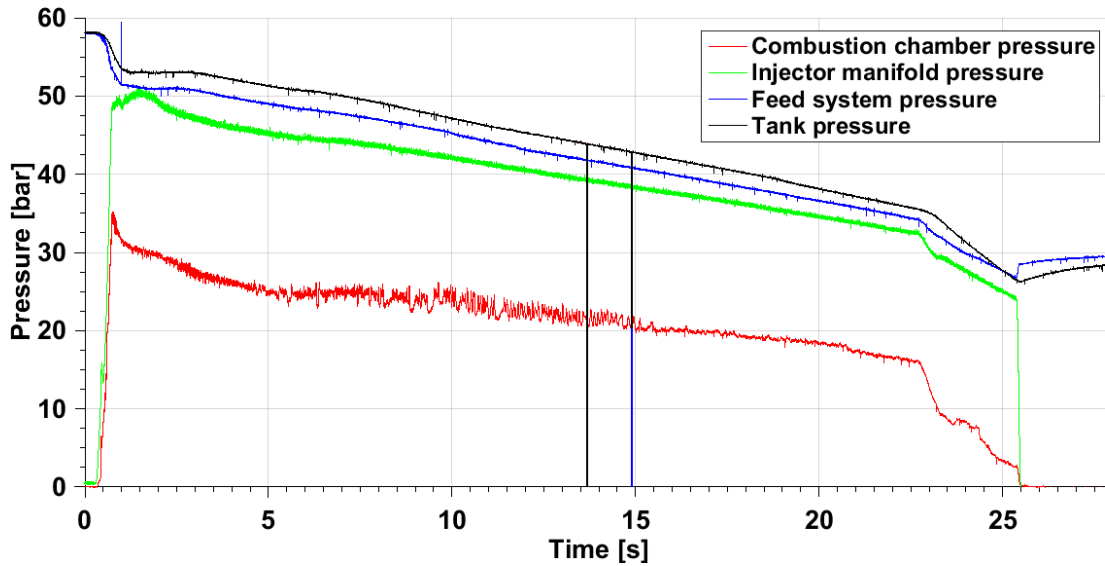


Figure 11: Pressure time trace for test 14 of combustion chamber, injector manifold, feed system and tank pressures

7 DISCUSSIONS

In this section the results as found in Sec. 6 are discussed. First an overview over the most interesting burns is given, including the changes implemented and a discussion of their effect. Test 14 is then discussed in detail to evaluate the achieved performance compared to the predicted.

Starting from the original baseline design, after the first test it was found out that the designed oxidizer mass flow was not met. The injector area was subsequently increased to allow for higher mass flows. This was only partially successful, as a choking point within the feed systems housing was identified later. O/F ratio and combustion chamber pressure could be raised as seen in Tab. 3. By removing the choking points in the system and with the increased area of the injector an initial oxidizer mass flux of $540 \frac{kg}{m^2s}$ was reached, which was below the design value of $600 \frac{kg}{m^2s}$. Due to the onset of problems at later tests the focus shifted towards mitigating these problems before increasing the oxidizer mass flow and flux. As the burn time of the initial burns was short a more accurate regression rate and therefore fuel mass flow for the liquid phase could be determined. This allowed to calculate the c^* efficiency of $\sim 75\%$ for this part of the burn and aided in identifying the improper mixing as mentioned in Sec. 4. As motors 3 and 4 failed the specific impulse could not be calculated due to the unknown amount of fuel used. The grain cracking in these motors has been traced back to entrapped air between the outer side of the grain and the inner side of the combustion chamber wall. By decreasing the

tolerances on the grain's outer diameter and by providing dedicated pressure equalisation ports this failure mode was mitigated. [8].

With the integration of the new mixing device the combustion chamber pressure was increased further to 30 bar. The overall system I_{sp} including the gaseous phase dropped marginally to 165 s. Due to this test the benefit of the new mixer could therefore not be conclusively seen from the specific impulse. Still it should be noted, that a drop in I_{sp} , compared to a fully liquid phase burn, was to be expected due to the gaseous blow down phase and the associated less optimal combustion. The total impulse was 98.2 kNs, which was caused by an incomplete filling of the run tanks to only 42.9 kg.

To build up on this test a series of tests was conducted over the full duration with completely filled tanks. During these tests a failure of the injector and subsequently the chamber close to the injector was encountered. At the time it was concluded to being caused by a heat insulation problem within this area. [8] Increasing the heat insulation in this area led to a partial success for test 10, where a failure was encountered close to the nozzle most probably caused by an improper assembly of the thrust chamber.

However, subsequent tests with a similar configuration were not able to cope with the heat fluxes experienced in the injector area. Strong fluctuations in thrust and combustion chamber pressure were noticed and analysis focused on these instabilities as a probable cause of excessive heating as suggest by [10]. By performing a fast fourier transform (FFT) on the sensor data,

it could be found that for the tests that failed at the injector a pronounced oscillation at around 450 Hz was present in the combustion chamber pressure and thrust. For unknown reasons this oscillation was very weak for tests 6 and 10. Oscillations have first been observed in test 2 after the oxidizer mass flux has been increased and were stronger with the new mixer design. A sample spectrogram of test 12 is given in Fig. 12.

Similar instabilities as seen in these tests were found in [14] and [3]. Based on this a flame holding instability is likely to have caused the instabilities. However, other causes, such as hydraulic flipping, or a combination of those could not be ruled out entirely. To mitigate the experienced oscillations, certain aspects of the design were changed. Most notably, for the next version the initial oxidizer mass flux was reduced from $540 \frac{kg}{m^2s}$ to $456 \frac{kg}{m^2s}$. In a previous effort to insulate the pre-combustion chamber from the excessive heat flux a phenolic ring with a thickness of 25 mm has been inserted. This ring was removed to reduce the area of the grain's top surface being covered by an ablator and to increase the volume of the pre-combustion chamber. It was intended for the changes to help in the formation of a vortex on top of the grain, through an increased volume. And to provide additional fuel for the vortex to burn and pre-heat the main oxidizer flow [6].

To protect the wall of the pre-combustion chamber a sandwich structure, consisting of an outside cardboard liner ring similar to the liner used for casting, a middle cardboard ring that is submerged into the fuel grain and an additional 3 mm cork ablator on the inside has been used. The final design is depicted in Fig. 1. All layers are glued together by high temperature silicone.

As can be seen in Fig. 10 the burn performed smoother than the burn for test 12, Fig. 9. This is verified by the spectrogram Fig. 13 which shows only very low powered and scattered oscillations at 450 Hz. The formation of strong oscillations in a narrowband around 450 Hz is missing. It can thus be concluded that the changes implemented helped to reduce the instabilities experienced at 450 Hz. Furthermore, as the excessive heating has not been experienced in this test, although, a thinner insulator has been used, the initial hypothesis of instabilities causing the increased heat flux is supported.

In Tab. 3 the outcome of test 14 and the design values are given. It is evident, that the main objective of achieving a total impulse of 177 kNs could not be met and it fell just 11.5% short of the design value of 200 kNs. However, the specific impulse could be slightly raised compared to the ISP of 195 s as measured during the fuel characterization studies [7]. While reducing the oxidizer mass flow rate it was found out that the regression rate of the fuel did not reduce in the same extent, thus shifting the O/F ratio to 2.8. This caused the fuel to

run out prematurely before all the oxidizer could be consumed. The gap in total impulse delivered can, therefore, be attributed to the lower amount of fuel used. As the O/F ratio operated at is below the ideal value of 3.3 it can be expected that the ISP will increase further by correcting the O/F ratio in the future. Increasing the oxidizer mass flow rate is also expected to increase the average chamber pressure and the average thrust, to be closer to the design value of 10 kN. Fig. 9 demonstrates the higher thrust level as achieved at higher mass flows.

8 CONCLUSIONS

A total of 14 static tests plus a flight test were performed on the DHX-200 Aurora, to evaluate and further increase its performance. These tests were conducted with two distinctively different motor designs, with the second design offering improved mixing. It was found with the first design that by increasing the oxidizer mass flux instabilities at around 450 Hz started to develop and to increase in intensity. The stabilities were further pronounced after switching to the second configuration. By lowering the oxidizer mass flux by 15% and redesigning the pre-combustion chamber to have more volume and a higher exposed fuel surface, it was possible to reduce these strong oscillations. Furthermore, when testing this configuration it was found that the heat flux at the injector side has been significantly reduced to not cause injector failure and that the specific impulse of the system was significantly increased, as well. It is, therefore, very likely that both have been caused by instabilities.

However, with the working configuration not all design goals could have been met. Decreased values were found for the total impulse, the average thrust, the average chamber pressure and the O/F ratio, while the specific impulse improved. The decreased performance can be attributed to the decreased oxidizer mass flow rate, through two different mechanisms.

Firstly, by lowering the combustion pressure, which in return lowered the average thrust produced.

Secondly, the O/F ratio was lowered, causing the fuel to burn up faster than expected, leaving a higher amount of unused propellant. With the specific impulse slightly increasing, the decrease in total impulse can be described by the lower amount of propellant used, as the impulse is linearly related to the specific impulse and the used propellant mass.

The initially low combustion efficiency could be increased through better mixing by the implementation of an improved mixing device. In the design process a CFD code was used to trade-off between different shapes of this device. As only a single shape has been tested it cannot conclusively be said that the predicted shape

indeed is the optimal shape. However, better mixing was achieved and thus the applicability of the presented CFD code to the DHX-200 Aurora could be shown.

The presented improvements on performance and stability have been paramount for the launch of Stratos II+ in October 2015. Through the described changes the motors performance and reliability could be raised for supporting that mission.

9 RECOMMENDATIONS

In the previous test series a lot of data on the DHX-200 Aurora and the effects of the described modifications could be gathered. Still, certain aspects could not be treated fully due to the limited amount of tests and the focus on progressing in the development of the motor. During the development full duration burns were needed for flight qualification. Unfortunately, due to the inability to measure fuel mass flow, important motor quality parameters could not be determined. Therefore, it would be recommended to perform a test series with short burns of around 2-3 s to properly evaluate the motors regression rate and its c^* efficiency. Measures on the change of regression rate with different oxidizer mass fluxes are of particular interest, as the mass flux needed to be changed to reduce instabilities, but caused a shift in O/F ratio that ultimately reduced the total impulse delivered. During these tests also different shapes for the mixing device can be tested to validate the CFD model and conclusively show the advantage of the mixing device.

Furthermore, the instabilities experienced in the design pose an interesting research subject. It is not completely known whether the instabilities are caused by flame holding issues or other causes like hydraulic flipping. Research in this field is not only interesting for understanding the motor better but also might show up possible solutions to dampen the instabilities at increased oxidizer mass fluxes. Additionally, it is very interesting to find out the cause for the instabilities of tests 6 and 10 to be weak. As it was seen that these weak instabilities still had a significant effect on the motors efficiency, further research could also lead increased performance by dampening oscillations at frequencies not considered in the original research.

To increase the impulse delivered of the motor, and meet its design requirements, the O/F ratio needs to be corrected. This can be achieved by tailoring the regression rate of the fuel through potential additives, or through an alternative way of treating the instabilities without lowering the oxidizer mass flow.

10 ACKNOWLEDGEMENTS

The authors would like to show their gratitude to the Technical University Delft and the TU Delft Space Institute, enabling this research through the student organization DARE. The sponsors of the Stratos II and Stratos II+ project. TNO and DLR for enabling the tests performed on a rocket motor of this size. National Instruments for providing assistance in the field of data acquisition and control.

REFERENCES

- [1] A. Bettella, M. Lazzarin, N. Bellomo, F. Barato, D. Pavarin, and M. Grosse. *Testing and CFD Simulation of Diaphragm Hybrid Rocket Motors*, 2011. AIAA 2011-6023.
- [2] Eric Doran, Jonny Dyer, Kevin Lohner, Zachary Dunn, Bryan Cantwell, and Greg Zilliac. *Nitrous oxide hybrid rocket motor fuel regression rate characterization*, 2007. AIAA 2007-5352.
- [3] A.B. Fraters. Flooding limit and flame holding instability in high mass flux hybrid rocket engines. *MSc. Faculty of Aerospace Engineering, Delft University of Technology*, 2014.
- [4] Arjan Fraters, Barry Zandbergen, Teun Weustink, Michael Eiche, Ingo Gerth, Rob Hermsen, Ralph Huijsman, Tobias Knop, Stefan Powell, and Ragiël Wildvank. *Development of a hybrid rocket engine for the Stratos II rocket*, 2011. IAC-11-C4.2.10.
- [5] Morteza Haghayegh. Launch campaign stratos ii day 9. *DARE Blog*, 6.10.2014. <http://dare.tudelft.nl/2014/10/launch-campaign-stratos-ii-day-9/>, last visited 20.03.2016.
- [6] J.E. Jones and R. A. Frederick. *Visualization of Recirculation Zones in Hybrid Rocket Motors*, 1996. AIAA 96-2842.

- [7] Tobias Knop, Ralph Huijsman, Stefan Powell, Robert Werner, Johannes Ehlen, Felix Lindeman, Jeroen Wink, Christoph Becker, Kapeel Samarawickrama, Barry Zandbergen, and Angelo Cervone. *Sorbitol-Based Hybrid Fuel Studies with Nitrous Oxide for the Stratos II Sounding Rocket*, 2013. AIAA 2013-4049.
- [8] Tobias Knop, Jeroen Wink, Ralph Huijsman, Stefan Powell, Robert Werner, Johannes Ehlen, Kapeel Samarawickrama, Barry Zandbergen, and Angelo Cervone. *Failure Mode Investigation of a Sorbitol-based Hybrid Rocket Flight Motor for the Stratos II Sounding Rocket*, 2015. AIAA 2015-4133.
- [9] M. Lazzarin, M. Faenza, F. Barato, N. Bellomo, A. Bettella, D. Pavarin, and M. Grosse. *CFD simulation of a Hybrid Rocket Motor with Liquid Injection*, 2011. AIAA 2011-5537.
- [10] G. P. Sutton and O. Biblarz. *Rocket Propulsion Elements*. John Wiley and Sons, 8th edition, 2010.
- [11] Mark Uitendaal. The stratos rocket – design, simulation and production of a record breaking rocket. Master's thesis, Delft University of Technology, July 2009. Master of Science thesis, Delft University of Technology.
- [12] Roel van der Heijden. Delftse studentenraket schiet naar recordhoogte. *Kennislink.nl*, 23.10.2015. <http://www.kennislink.nl/publicaties/delftse-studentenraket-schiet-naar-recordhoogte>, last visited 20.03.2016.
- [13] Jeroen Wink, Tobias Knop, Ralph Huijsman, Stefan Powell, Kapeel Samarawickrama, Arjan Fraters, Robert Werner, Christoph Becker, Felix Lindeman, Johannes Ehlen, Angelo Cervone, and Barry Zandbergen. *Test Campaign on a 10 kN class Sorbitol-Based Hybrid Rocket Motor for the Stratos II Sounding Rocket*, 2014. SP2014-2969362.
- [14] Greg Ziliac, Benjamin Waxman, Jonny Dyer, M. Arif Karabeyoglu, and Brian Cantwell. Peregrine hybrid rocket motor ground test results. *48th AIAA/ASME/SAE/ASEE Joint Propulsion Conference*, 2012. AIAA 2012-4017.